The Structure of Protoplanetary Gas Envelopes in Isothermal Hydrostatic Equilibria

Author: Amin Uddin Ahmed
Supervisor: Dr Sijme-Jan Paardekooper

Queen Mary University of London,
School of Physics and Astronomy
Mile End Rd, London E1 4NS, UK

In this project we use the nucleated instability model of giant planet formation to model the internal structures of gas giants, at hydrostatic and quasi-hydrostatic equilibria in a gaseous circumstellar nebula at a distance of 5.2 AU from the star. The protoplanet is modelled as spherically symmetric, composed of a smooth, solid non-porous core of uniform density surrounded by an isothermal ideal gas envelope that extends upto the hill sphere, with a fixed density at the core surface which decreases as one ascends further away from the core. The simulation is executed without stipulating any final planet mass, but only using the initial conditions of core mass and surface density, allowing us to arrive at a wide range of hydrostatic envelope equilibria by permitting a natural progression of the simulation. We find that there are two types of envelope equilibria: a smooth equilibria at lower surface densities, and a sharp equilibria at high surface densities. We find that there are a minimum of two solutions for any core in a set nebula, at masses less than the global critical core mass. The critical masses for a core with standard mass and radius are found to be 2.3×10^{22} and 1.2×10^{23} kg, both at a surface density of $\approx$ 500 kg m^{-3}. The critical masses for an extended core radius of 64 times the initial radius are found to be 8×10^{21}, 7×10^{24}, and 4×10^{25} kg at surface densities of $\approx$ 2, 0.005, and 0.01 kg m^{-3} respectively. We conclude that extending the core radius allows a much larger range of both local and global static critical core masses, which are found at much lower surface densities.

Contents

1 Introduction

In recent years the discovery of extrasolar planets have grown exponentially (*1*), and demand for understanding more about the newfound planets is increasing every day. One major aspect of understanding a planet is to be able to accurately describe both its internal and external structure.

From observation, it has been found that large gas giant planets can be found in a huge range of distances from their parent star, in some cases with orbital periods of less than a day (*2*) (commonly referred to as hot jupiters or roaster planets), to others with orbital periods of thousands of years (*3*). The huge variety in the sizes, orbits, and structures (*4*) means there is so much more to be learnt about forming planets, and while much research is currently taking place, there are still significant gaps in our knowledge of planet formation.

While much research has been conducted in this field, there are still many more aspects that require further study. And as we learn more about protoplanetary systems, new questions and problems constantly present themselves, and in the process of solving those, new ideas and theories which can be explored.

One of these new problems is a thorough investigation of a wide range of protoplanetary hydrostatic models in order to investigate the variation of the outer density with respect to the surface gas density, which will then allow us to determine the critical core mass of a forming giant gas planet. Furthermore, investigating how the critical mass is affected by changes to the core density and radius.

One model that has been presented for planetary formation is that when a rocky core is embedded in a gaseous nebula, it slowly attracts gas from the surroundings until it reaches a point known as the critical mass. When the core mass is greater than the critical mass, it enters a phase of *rapid gas accretion* where it begins to capture huge quantities of gas from the circumstellar disk, and forms a giant gas planet (*5*), (*6*). Knowing the critical core mass is key to determining the mass the planet will be when formation is complete.

When attempting to create a three-dimensional model of a forming planet is that simply extrapolating the spherically symmetric radial model to three dimensions will require tremendous amounts of computational power to retain the resolution. Therefore, an adaptation to the model is necessary.

A problem that is found when trying to numerically simulate a three-dimensional model of a protoplanetary structure is that when splitting the spherical space into ”boxes”, there is an infinite potential at the very centre, where the core is. Thus we must construct what can be described as a ”softened potential”, where the core is modelled as having the same mass but a

much larger radius, in order to avoid the infinite potential at the centre. Investigation is required to find out how such a modification to the physical system will affect the critical mass of the planet. This is the aim of this project.

1.1 Formation of Giant Planets

There are two main models of giant gas planet formation and much research is being done to investigate the applicability of each. A brief description of each model is given below.

1.1.1 Core Accretion

In a solar system nebula formed of rocks and gas, initially solid rocky matter collides and some of these collisions result in the rocks sticking together (pebble accretion phase) (*7*). As the clump of rocks gets larger, the forming core has a greater gravitational range, allowing it to pull matter from further out. Initially, gas slowly accretes onto the core (slow envelope accretion phase), until it reaches a critical mass that triggers gaseous runaway growth (*8*): where gas accretes onto it at a very fast rate (rapid gas accretion phase). This process is also called the Nucleated Instability model, as it is dependant on a solid rock and/or ice 'nucleus' forming prior to any gas envelope. (*9*)

1.1.2 Gravitational Instability

In a realistic circumstellar nebula, the distribution of matter is not perfectly uniform, i.e. some regions have slightly higher densities than others. These regions have a stronger gravitational pull on the surrounding matter, which results in the gas nebula around the star splitting itself apart into clumps of matter via self-gravitational effects. As the perturbations become more pronounced, these clumps (referred to as Giant Gaseous Protoplanets) (*10*) then continue to collapse and contract due to gravity until it becomes a fully formed planet. It has been observed that the giant gaseous protoplanets tend to arrange themselves into a spiral formation (*11*). These spiral arms then fragmenting and collapse into the planet (*12*) (*13*).

2 Simulation Model

2.1 The Nebula

We model the protoplanet as having a circular orbit around the central star, which has been fixed to one solar mass. The protoplanet orbit has been fixed to 5.2 AU (which is in a common region for many gas giants (*14*)), this will ensure that the gravitational pull from the sun (and thus the protoplanet hill sphere) is kept constant, as well as the equilibrium temperature of the gaseous envelope.

2.1.1 Properties of the Gas

The nebula in which the giant planet envelope forms in (and is made from) is modelled as a uniformly distributed classical (Maxwell-Boltzmann) ideal gas with an equation of state (*19*):

$$PV = nRT \tag{1}$$

where P is the pressure, V is the volume, n is the number of moles of the gas, R is the universal gas constant, and T is the temperature. As a result of this, we ignore any intermolecular forces between the gas particles, and the volume of the atoms themselves are disregarded i.e. point masses.

The gas is set to have a mean molecular weight of $\mu = 2.3 \times 10^{-3}$ kg m^{-3}. This envelope will also be static, as we are only investigating the structure as a fixed point in time, without any time evolution.

2.1.2 Equilibrium Temperature

According to the Stefan-Boltzmann Law, the power that is radiated out of a black body is given by: $P = \sigma A T^4$. Assuming that the planet is a perfect sphere with no tidal stretching, the power emitted by the planet is:

$$P_{out} = 4\pi R_p^2 \sigma T_{eq}^4 \tag{2}$$

Where P_{out} is the power emitted by the planet, R_p is the planet radius, σ is the Stefan-Boltzmann constant, and T_{eq} is the equilibrium temperature.

On the other hand, the power that is received by the planet is described by the power output of the parent star (i.e. the luminosity), divided by the solid angle the planet takes up in the "sky" of the star - effectively the fraction of the light that is received by the planet:

$$P_{in} = L_*(1-a)\sqrt{\frac{\pi R_p^2}{4\pi D^2}} \tag{3}$$

Where P_{in} is the power radiated onto the planet by the star, L_* is the luminosity of the star, a is the albedo (fraction of light reflected by the planets atmosphere), R_p is the planets radius, and D is the distance between the planet and the star.

In our model, we ignore the effects of light reflected by the gas envelope (albedo = 0), to keep our equilibrium temperature consistent with the value in the model used by *(Pečnik and Wuchterl)* (*18*). We also ignore the greenhouse effect and any radiative forcing by the gas envelope.

By setting $P_{in} = P_{out}$ and rearranging for T_{eq}, we get the equilibrium temperature as:

$$T_{eq} = T_*\sqrt{\frac{r_*}{2d}} \tag{4}$$

Where T_* is the surface temperature of the star, r_* is the stars radius, and d is the distance between the star and the planet.

An interesting point to note is that when equating P_{in} to P_{out}, the planets radius cancels out - this results in the equilibrium temperature depending only on the distance from the parent star and the stars properties. Effectively, an object or body of any size will have the same equilibrium temperature, provided the distance from the parent star is equal. This means that protoplanets of various sizes all have equal temperature.

With the distance fixed to 5.2 AU and using the surface temperature of our sun as 5800 K, the equilibrium temperature of our circumstellar nebula at this distance is 122.67 K. We assume this temperature is preserved throughout the protoplanet gas envelope, ignoring any heating induced by pressure.

2.2 Planetary Hill Sphere

The Hill Sphere of a body is the region in which it exerts the dominant gravitational pull upon all other objects, meaning that things will be attracted or fall towards it instead of away. The Hill Radius of a body with respect to another body is given by:

$$R_{hill} = a\sqrt[3]{\frac{M_p}{3M_*}} \tag{5}$$

Where a is the semi major axis, M_p is the mass of the secondary (our protoplanet), and M_* is the mass of the primary (our star).

In our model, this is important as it gives us an outer boundary for the gas that can accrete onto it from the planetary nebula. Any gas further away that this region will instead orbit the star itself. Others have instead used what is known as the Bondi radius (*15*) to establish an accretory boundary, which is derived by equating the speed of sound in the nebula to the planets escape velocity (*16*):

$$c_s = v_{esc} = \sqrt{\frac{2GM_p}{r}} \tag{6}$$

Where c_s is the speed of sound, v_{esc} is the escape velocity, M_p is the mass of the planet, and d is the distance from the planets centre of mass. This is then rearranged to:

$$R_{bondi} = \frac{GM_p}{c_s^2} \tag{7}$$

Another numerical model has arrived at what can be described as a "modified" hill radius (*17*), where the experiment demonstrated that not all of the protoplanetary nebula gas that passed through the full hill radius actually accreted onto the planet, but rather a significant portion flowed past the protoplanet. This new effective hill radius is given by:

$$R_{eff} = \frac{GM_p}{c_s^2 + \frac{4GM_p}{R_{hill}}} \tag{8}$$

Which was found to be approximately a quarter of the original hill radius (*17*).

With the orbital distance fixed to 5.2 AU, an initial core of one earth mass, and the star being one solar mass, the initial Hill Radius of the protoplanetary core is 7.504 10^9 m.

2.3 The Protoplanetary Core

We initially model the protoplanetary core as being a solid non-porous uniform rocky sphere of fixed density ρ_{core} = 5500 kg m^{-3}. The mass of the core is given by the volume of the sphere multiplied by the density:

$$M_{core} = \frac{4}{3}\pi r_{core}^3 \rho_{core} \tag{9}$$

where M_{core} is the mass, r_{core} is the radius of the core, and ρ_{core} is the core density.

2.4 Hydrostatic Equilibria Equations

The mass equation for a sphere in differential form, as the density is non uniform:

$$\frac{dM(r)}{dr} = 4\pi r^2 \rho(r) \tag{10}$$

From the equation of hydrostatic equilibria:

$$\frac{dP}{dh} = -g\rho \tag{11}$$

Since we are dealing with large distances, over which the gravitational acceleration will not remain constant, we must use the equation:

$$g = \frac{GM}{r^2} \tag{12}$$

and substituting in the gravitational acceleration, and letting the height be the radius from the core surface, we get:

$$\frac{dP(r)}{dr} = -\frac{GM(r)\rho(r)}{r^2} \tag{13}$$

We modify the ideal gas law (Equation 1) to represent the pressure in terms of the atomic mass of the gas, and the density at some distance from the core.

$$P = \frac{RT\rho(r)}{\mu} \tag{14}$$

$$\frac{dP(r)}{dr} = \frac{RT}{\mu}\frac{d\rho(r)}{dr} \tag{15}$$

$$\frac{d\rho(r)}{dr} = \frac{G\mu}{RT}\frac{M(r)\rho(r)}{r^2} \tag{16}$$

On thing to note, is that since we have a solid core as opposed to a pure ball of gas in space, we define the total mass of the protoplanet as the sum of the solid and gaseous components:

$$M_{tot} = M_{core} + M_{env} \tag{17}$$

2.5 Boundary Conditions

We assign the limits for the gaseous envelope:

The minimum will be the core surface, where it is physically impossible for any gas to inhabit, as the core is modelled as a non-porous solid:

$$R_{min} = R_{core} = \sqrt[3]{\frac{3M_{core}}{4\pi\rho_{core}}} \tag{18}$$

The maximum will be the hill radius, as any gas outside this boundary will be outside the sphere of influence of the forming planet, and thus will be considered part of the protoplanetary nebula:

$$R_{max} = R_{hill} = a\sqrt[3]{\frac{M}{3M_*}} \tag{19}$$

2.5.1 Recalculation

Since the actual hill sphere of our forming planet is dictated by the total mass, as opposed to just the core mass (i.e. we have a non trivial gas envelope mass), the actual hill radius will change as we ascend further above the surface. This recalculation is based on Equation 19 and what we define the total mass to be (Equation 17),and repeating this calculation every time we take a step in the radial direction.

$$R_{hill} = a\sqrt[3]{\frac{M_{tot}}{3M}} \tag{20}$$

2.6 The Solution Algorithm

2.6.1 Eulers Method

Given a standard simple differential equation:

$$\frac{dy}{dx} = f(x, y), \qquad y(x_0) = y_0 \tag{21}$$

We can pick a step size h and compute the y value at the next point by adding the difference between x_n and x_{n+1} with the following equation:

$$y_{n+1} = y_n + hf(x_n, y_n) \tag{22}$$

Which can also be expressed as:

$$\Delta y = f(x, y)\Delta x \tag{23}$$

In our specific case, the density and mass equations are respectively given by:

$$\Delta\rho(r) = \frac{G\mu}{RT}\frac{M(r)\rho(r)}{r^2}\Delta r \tag{24}$$

$$\Delta M = 4\pi r^2\rho(r)\Delta r \tag{25}$$

And we can thus calculate the envelope density and mass at a radius r_{n+1} by adding the change in density $\Delta\rho(r)$ and the change in mass ΔM to the previous values at a radius r_n

2.6.2 Runge-Kutta Method

When utilising the Euler method it was found that the values were wildly fluctuating near the core surface, in some places even resulting in negative densities and mass. This was due to the density falling off particularly rapidly at the core surface, and at extremely high density changes within a small radial step, resulted in ”overshooting” the solutions, with subsequent steps normalising the curve eventually, as the changes in density became smaller.

An early attempt to remedy this was to reduce the stepsize to eliminate the overshooting issue, however it was found that in order to get a reliable and accurate graph we required to compute in excess of 10^8 points, which was computationally unfeasible. Thus, we had to look into higher order methods of solving ordinary differential equations numerically.

The Runge-Kutta 4th order equations (*20*) are as follows (Equations 26-31), with h being the stepsize, and k_{1-4} being intermediary solutions, all of which are assigned weights and then

summed up to give a far more accurate solution. Furthermore, to increase precision, a factor of 2 increase in the step size resolution reduces the solution error by 32, or an n factor decrease in the step size results in n^5 decrease in error.

$$x_{n+1} = x_n + h \tag{26}$$

$$y_{n+1} = y_n + \frac{h}{6}(k_1 + 2k_2 + 2k_3 + k4) \tag{27}$$

$$\begin{aligned} k_1 &= f(x_n, y_n) && (28)\\ k_2 &= f(x_n + \frac{h}{2}, y_n + \frac{h}{2}k_1) && (29)\\ k_3 &= f(x_n + \frac{h}{2}, y_n + \frac{h}{2}k_2) && (30)\\ k_4 &= f(x_n + h, y_n + hk_3) && (31) \end{aligned}$$

3 Results

3.1 Mass Profiles

From the Figures 1 and 2 we can determine two different models to describe the structure of giant protoplanets.

In Figure 1 the mass of the envelope is growing exponentially as we ascend from the radius, indicating that the volume increases faster than the density decreases. This would be aptly described as a *smooth* envelope, where the density is relatively stable through the envelope. Also as can be noticed, is that the total mass does not increase by a significant amount - i.e. the envelope mass is much smaller than the core mass. This is indicative of particularly low core surface densities.

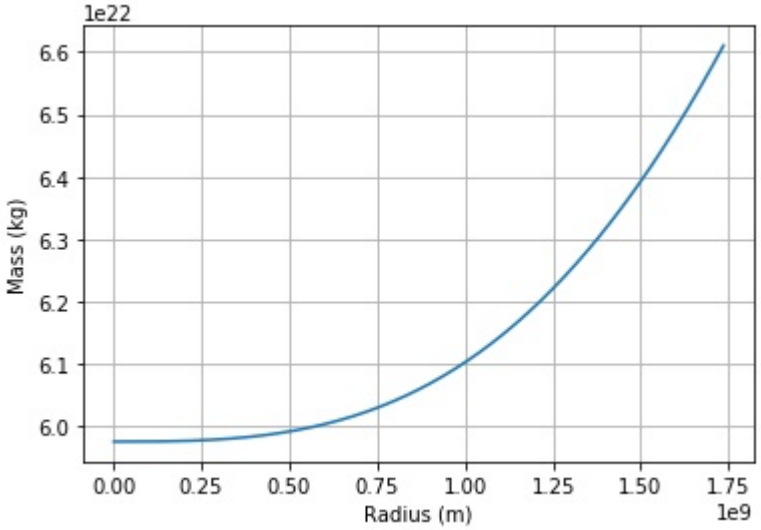

Figure 1: Mass profile of a protoplanet with a surface gas density of 2.1 10^{-4} kg

In Figure 2 the total mass of the protoplanet increases very sharply within a short distance, then stabilises. This can be described as a *sharp* envelope, where within a short distance there is a very dense layer of gas which acts very similar to the core itself, in regards to the gravitational effects on further gas accumulation from the nebula which is visible in Figure 5. This effect is even more pronounced at even higher core surface densities.

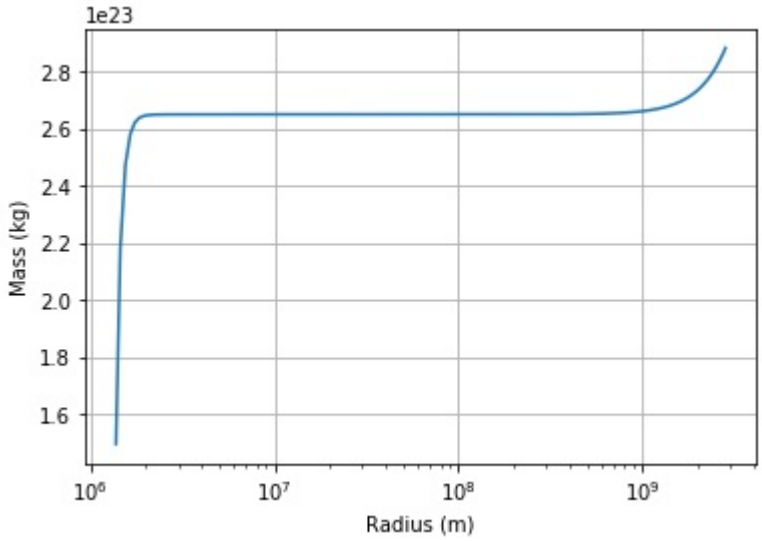

Figure 2: Mass profile of a protoplanet with a core surface gas density of 7.9 10^4 kg

3.2 Density Profiles

Figure 3 shows the density profiles (internal envelope structure) of a planet of mass 0.01 $M_{\oplus}$ for the solutions belonging to a nebula with a gas density of 10^{-6} kg m^{-3}. We see the density profiles of 6 envelopes, each one in hydrostatic equilibrium with the surrounding nebula. The profiles for the surface densities can be seen to form pairs, each stabilising at a particular density for a region within the gas envelope, until eventually falling to the nebula density on the outer boundary; at 10^{-6} kg m^{-3}. These pairs also correspond to the most dense matching with the least dense surface, the second highest density with the second lowest density, etc. This is better visualised in Figure 9 where the solutions clearly follow contours, until converging at a critical mass.

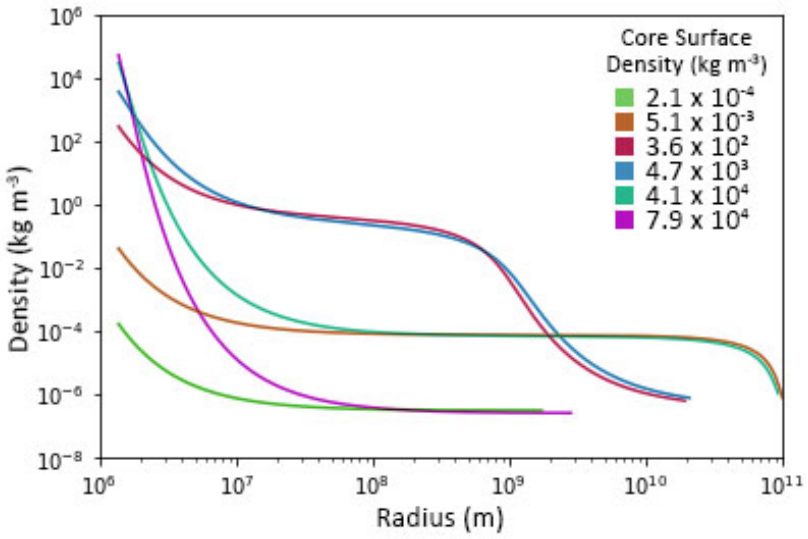

Figure 3: The density profiles of gas envelopes that have a core surface density corresponding to the solutions in Figure 7.

3.3 Hill Spheres

As we observe in the Figures 4-5, lower density surface gas will result in an exponentially increasing hill sphere as we ascend from the core, while a very dense gas at the core surface will cause a sharp rise in the total mass (see Figure 1) and thus the hill radius in a relatively small distance from the surface. At a surface density of approximately 10^{-2} kg m^{-3}, the relation between radius and the hill sphere is linear. This supports the concept of an *effective core mass* at high surface densities, as the hill sphere levels out within a short distance. This is key to explaining the global critical core mass.

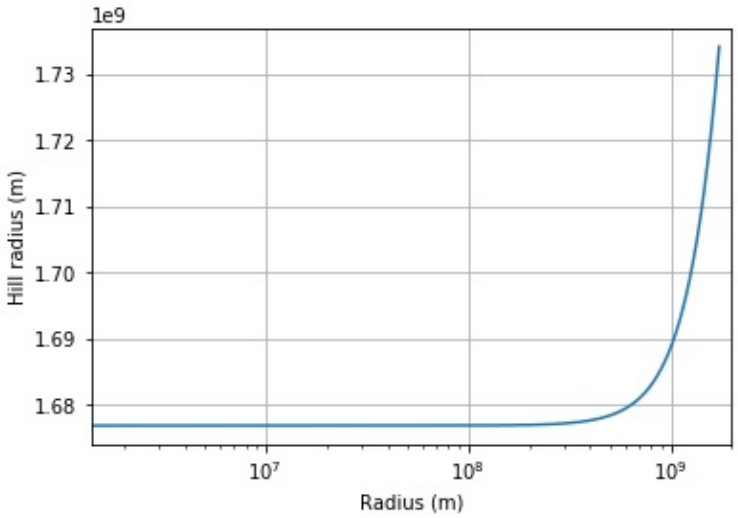

Figure 4: The change in the hill radius with respect to the radius from the center, of a core surface density $\rho_{csg} = 2.1 \times 10^{-4}\ kg\ m^{-3}$

3.3.1 Effective Core Mass

The effective core mass is predominantly found to exist in cases of particularly high core surface density, especially where $\rho_{csg} > \rho_{core}$. At such high surface densities there is a significant jump in the total mass (see Figure 2) in a short distance, and therefore also the gravitational pull on the nebula. Thus, the thin layer of very heavy gas in the envelops behaves as it were part of the core itself, at least in the regards of how it affects the collection of more gas from the nebula. In such cases, it is observed that there is a very sharp density falloff very close to the core: see Figure 3, the turquoise and purple lines corresponding to surface densities of 4.1×10^4 and 7.9×10^4 kg m^{-3} respectively.

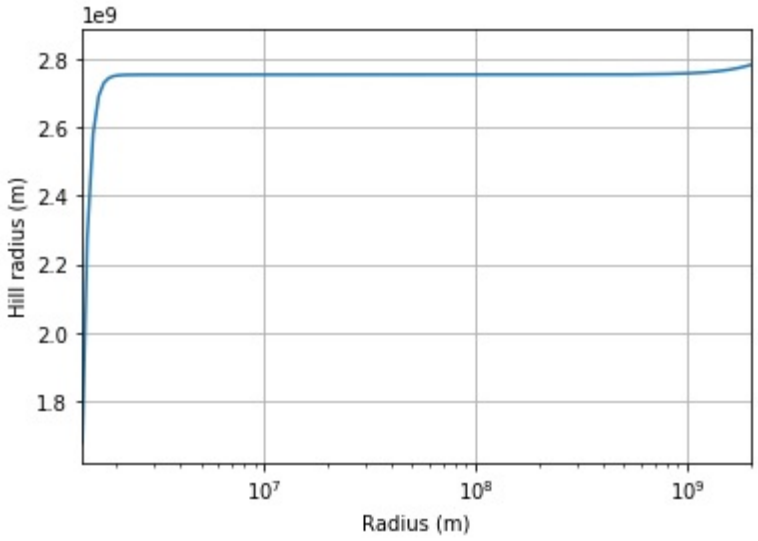

7-9e4.jpg

Figure 5: The change in the hill radius with respect to the radius from the center, of a core surface density $\rho_{csg} = 7.9 \times 10^4\ kg\ m^{-3}$

3.4 Solution curve for outer densities

The points at which the outer density intersect with the orange line (Figure 7) are in hydrostatic equilibria with a protoplanetary nebula with a density of 10^{-6} kg m^{-3}. There are six solutions, one for each intersection. These six solutions can be grouped into three pairs of solutions, where the densities within the internal envelope structure match for a large portion of the envelope. A demonstration of this is in Figure 3. A more detailed explanation for this phenomenon is described in Section 3.2.

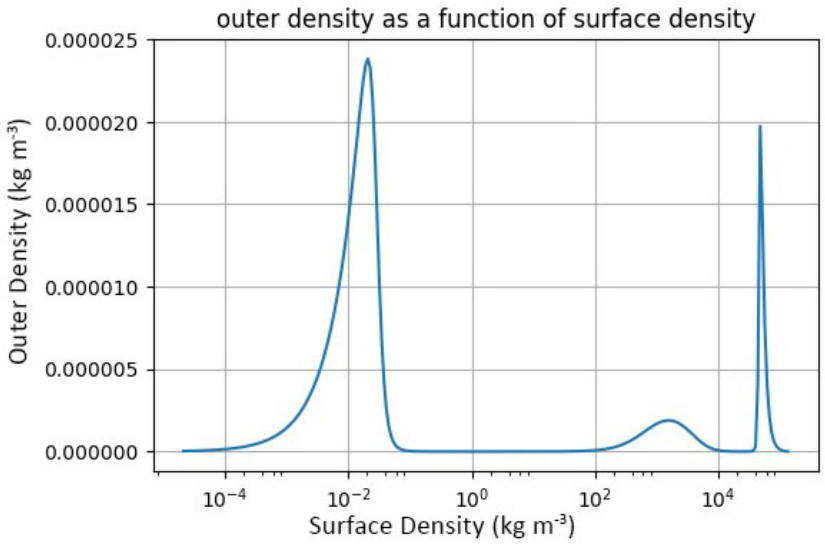

Figure 6: The envelope outer density against the gas density at the core surface, where M_{core} = $0.01M_{\oplus}$ = 5.976 10^{22} kg.

Figure 8 demonstrates how the outer density against the surface density evolves as the core varies in mass. The critical core mass is found as the mass at which the peaks of the outer density match the protoplanetary nebula density. See Figure 3 for a visual representation of this.

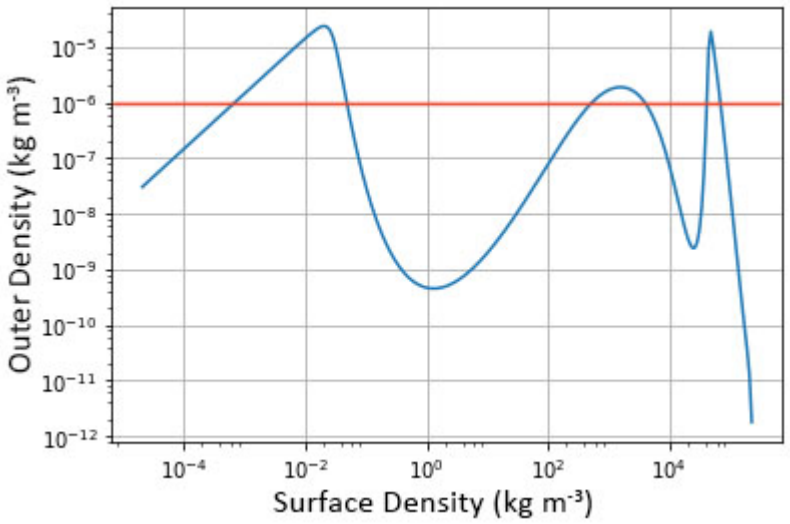

Figure 7: Logarithmic graph of the envelope outer density against the gas density at the core surface, where $M_{core} = 0.01 M_{\oplus} = 5.976 \times 10^{22}$ kg.

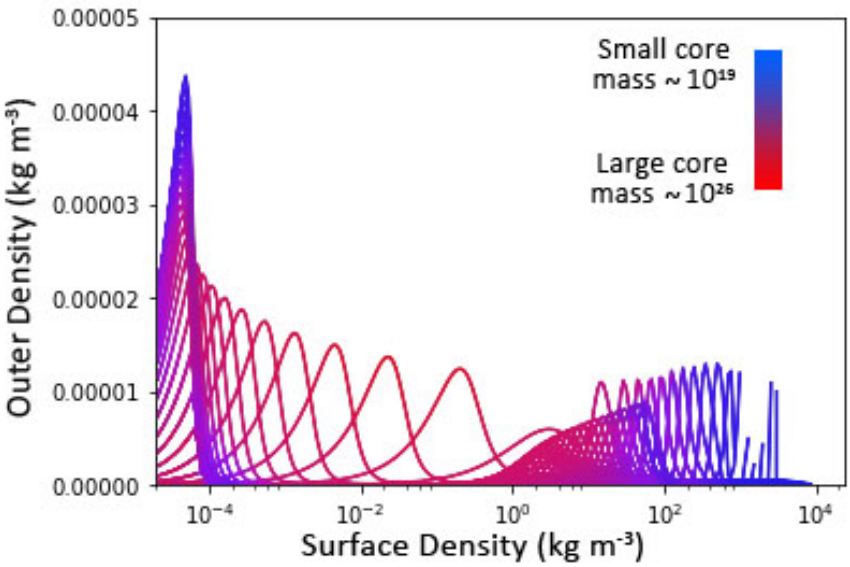

Figure 8: Graph showing the outer densities with respect to surface densities of 34 different cores, ranging from 10^{19} to 10^{26} kg.

3.5 Critical Mass

The critical mass is the point most to the right of the graph. As can be seen, there is a local critical core mass at 2.3 $\times$ 10^{22} kg, and a global critical core mass at 1.2 $\times$ 10^{24} kg, both at outer densities of 500 kg m^{-3}.

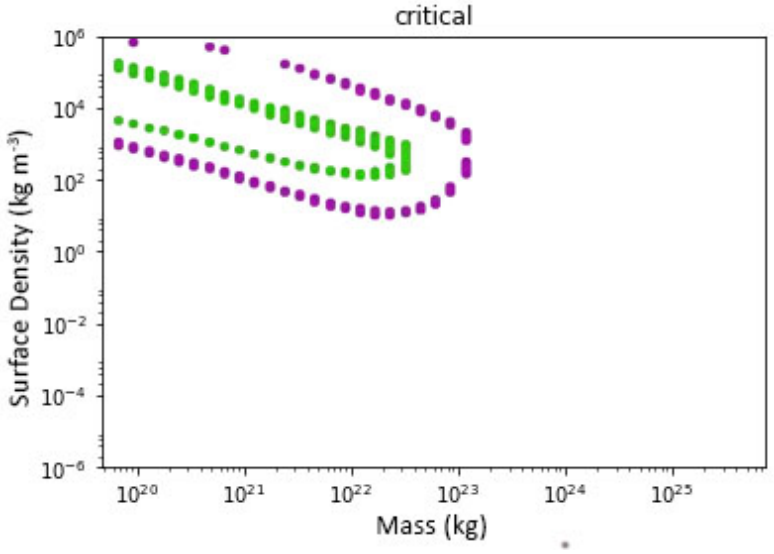

Figure 9: The solution branches of an outer nebula of 10^{-6} kg m^{-3} with a radius of 6.377 $\times$ 10^{6} m.

3.6 Effects of enlarging the core

It is observed that the local and global critical core masses are shifted further out into the region of higher masses, at 7 $\times$ 10^{24} kg and 4 $\times$ 10^{25} kg. Also, another local critical mass begins to appear, at 8 $\times$ 10^{21} kg. Interestingly enough, the solution branch is not contained within the branch for the next local critical core mass, but is separate. This phenomenon has been observed in the simulations by B. Pecnik and G. Wuchterl (*18*), however to date there is no known explanation.

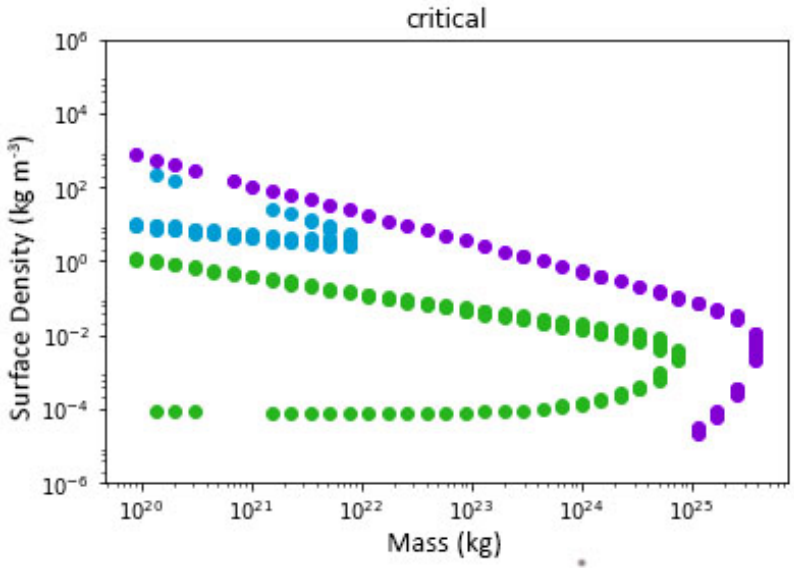

Figure 10: The isobaric solution branches of an outer nebula of 10^{-6} kg m^{-3} with an extended radius of 4 $\times$ 10^8 m (64 $R_\oplus$) indicating the critical core masses.

4 Discussion and Conclusions

There are many factors that can affect the results attained, and a significant contribution of that is the assumptions made at the start. The conditions dictating the simulations are vastly simplified in order to streamline the process.

For example, the ideal gas equation was used as opposed to the Van der Waals equation of state. This ignores the effect of the volume taken up by the atoms themselves, instead approximating them as point masses. Also, intermolecular forces between the gas molecules have been disregarded. These two effects would normally have a non-trivial effect on both the temperature and pressure of the envelope - effectively making the effect of gravity more significant, and thus giving values for the critical mass that are smaller than they really should be.

Another significant factor is that the nebula was not modelled to have a finite quantity of gas, or deplete in any way. The density remained constant throughout the planets formation. Adding in this limitation would result in smaller planets and envelopes. Furthermore, the distance was fixed to 5.2 AU as a circular orbit, under normal conditions a slight eccentricity would result in a larger "range" of gas to accrete. This would have resulted in larger planets being formed.

One other significant contributor is the computational power available, and the simplifications that had to be done in order for feasibility. In fact, this whole paper is the investigation of a method used to make a three dimensional simulation of a forming planet computationally feasible. Amongst others, this includes the limited number of masses, densities, cores, and nebulae that could be investigated. Also, the resolutions for many aspects of the algorithm had to be adjusted, such as the radial increments, the number of iterations for the density calculation, and the range of cores to model. The results attained could perhaps be substantially different were the resolutions increased.

The envelope equilibria can be separated into two categories, as can be seen in Figure 3:

A *smooth* envelope where the density falloff is mild from the core surface to the envelope edge - usually within two orders of magnitude. This type of envelope is commonly found where the surface density is relatively low.

A *sharp* envelope where there is a very sharp drop in gas density spanning many orders of magnitude close to the core surface. This envelope profile is generally attributed to high core surface densities.

For a core that is lighter than the critical mass, we always have a minimum of two gas envelope solutions for a predefined protoplanetary nebula. The critical core mass is at the point where the higher and lower density solutions converge.

In a fixed density protoplanetary nebula, the local and global static critical core masses are

found to be significantly larger as a consequence extended core radius, becoming many times larger than an earth mass - whereas under normal core conditions the largest attainable core mass is an order of magnitude smaller than the mass of the earth. Also, these new critical cores are achieved with a much lower envelope density at the core surface. This indicates that a large-core approximation when extending the one dimensional simulation to three dimensions would yield significantly different critical mass values, and as a direct consequence different planetary formation models.

References and Notes

1. E. Deems, L. Fletcher, B. M. Levine, G. Orton, G. Vasisht .
2. C. Hellier, *et al.*, *Nature* **460**, 1098 (2009).
3. C. Scharf, K. Menou, *The Astrophysical Journal Letters* **693**, L113 (2009).
4. B. S. Gaudi, *Bulletin of the American Astronomical Society* (2010), vol. 42, p. 452.
5. A. P. Boss, *The Astrophysical Journal Letters* **536**, L101 (2000).
6. J. B. Pollack, *et al.*, *icarus* **124**, 62 (1996).
7. J. E. Chambers, *The Astrophysical Journal* **825**, 63 (2016).
8. O. M. Guilera, *BAAA* **58**, 63 (2016).
9. H. Mizuno, *Progress of Theoretical Physics* **64**, 544 (1980).
10. A. P. Boss, *Science* **276**, 1836 (1997).
11. D. R. H. et al, *Protostars and Planets Vl* **436**, 607 (2007).
12. A. P. Boss, *Science* **276**, 1836 (1997).
13. G. Laughlin, P. Bodenheimer, *The Astrophysical Journal* **436**, 335 (1994).
14. E. W. Thommes, M. J. Duncan, H. F. Levison, *Icarus* **161**, 431 (2003).
15. H. Bondi, *MNRAS* **112**, 195 (1951).
16. G. Khatri, Poudel, *Kathmandu, Ayyam Publication* pp. 170, 171 (2010).

17. Y. Greenzweig, J. J. Lissauer, *Icarus* **100**, 440 (1992).

18. B. Pecnik, G. Wuchterl, *Astron. Astrophys.* **440**, 1183 (2005).

19. É. Clapeyron, *Mémoire sur la puissance motrice de la chaleur* (J. Gabay, 1834).

20. J. R. Dormand, P. J. Prince, *Journal of computational and applied mathematics* **6**, 19 (1980).